Available online www.jsaer.com

***Journal of Scientific and Engineering Research*, 2023, 10(3):17-33**

Research Article

ISSN: 2394-2630
CODEN(USA): JSERBR

Homotopy Solution of Temperature and Induced Magnetic Field Effects on MHD Convective-Diffusive Nanofluid Flow over a Stretching Wedge

Olufemi A. Akinyemi[1], Raphael E. Asibor[2], Akindele M. Okedoye[1, 3]*

[1]Department of Mathematics, College of Science, Federal University of Petroleum Resources, Effurun, Nigeria
[2]Department of Computer Science/Mathematics, Igbinedion University Okada, Edo State, Nigeria
[3]Department of Mathematics, College of Science and Technology, Covenant University, Canaan Land, Ota, Nigeria
*Corresponding author: okedoye.akindele@fupre.edu.ng

Abstract The effect of heat source and thermal buoyancy on Induced Magnetic Field Nano-Fluid over a Stretching Wedge with Slip was investigated. The problem is modeled into a system of coupled non-linear partial differential equations. The radiation heat flux is taken in the form of a unidirectional flux in the y direction. A stream function is used to transform the system to a set of ordinary differential equations. The resulting ordinary differential equations was solved using Homotopy Analysis Method that uses the homotopy parameter that split nonlinear system into an infinite set of linear systems which are solved analytically, while the continuation methods require solving a discrete linear system as the homotopy parameter is varied to solve the nonlinear system. The result of the procedure is represented both in figures and tables, some of the result obtained indicates that, velocity increases as stretching velocity increases, at a higher stretching velocity, velocity close to the surface is higher that the velocity at the surface. Stretching velocity decreases the concentration, that when heat moves from solid surface to fluid the temperature of the fluid flow increases, that slip velocity increases skin-friction and Nusselt number and decline Sherwood number of the flow field, Increases in Suction velocity decreases skin-friction and Nusselt number, while increases in Nanofluid parameter increases the skin friction and Nusselt number. The inclusion of induced magnetic field and higher order chemical reaction makes it interesting and useful for applications in the space technology, metallurgy, and pharmaceutical engineering industries, such as food processing technology, various hospital treatments, and polymer production.

Keywords Induced Magnetic Field, Nano-Fluid, Stretching Wedge, Slip velocity, radiation, heat flux. thermophoresis

1. Introduction

Flow fluids that are influenced by convection are frequently encountered in solar power receivers, electronic appliances, cooling systems, and drying processes. Free convective flow is characterized by linear density difference embodies buoyant forces [1];[2]. The flows occur in an extensive range of natural circumstances and industrial applications, as in oil recovery, aquifer pollutant dispersion, and agricultural water circulation. Earlier experimental and theoretical work on convective flow was performed by [3], [4],[5], and [6]. Convective flows support mixing and stirring mechanism of heterogeneity chemical reaction with stretching component which takes place in an occurrence of velocity gradient [7].[8] utilized natural convection to induce buoyancy flow on the bounded flow of nanomaterial in a vertical medium. The flow was strongly influenced by buoyancy convective forces and stretching velocity.[9] examined convective stagnation nanofluid flow past a stretching device using series analytical solution. It was noticed that the flow reaction mixture was propelled by thermal buoyant force.

Fluid properties and its usefulness can be improved by magnetic induction that create electrical conductivity of the fluid, and have been applied in magnetohydromagnetic (MHD) power generators, nuclear reactors, heat exchangers and many other processes [10]. [11] inspected magnetic field impact on the nanofluid boiling subcooled flow. The fluid viscosity was encouraged with rising magnetic field effect. [12] obtained computational results for boundary layer laminar wedge MHD flow with heat generation and radiation. The conduction fluid flow rate was resisted by increasing the magnetic term. Other studies on the convective magnetic fluid flow were performed by [13], [14],[15], and [16].

Flow fluids involving radiative heat and heat absorption or generation phenomena are of increasing interest because of their use in mechanical and computer technologies. Radiation and heat sink or source changes heat distribution that affect the system rate of particle deposition [17]. These quantities progressively boost fluid temperature due to changes in the intermolecular collision as found nuclear reactor technology and electrolyte battery production [18]. Due to the importance of the quantities, [19], [20] examined combined convective furnace and free-radiation for a boundary designed problem. A volume finite technique is used to solve the radiative heat and flow momentum equations.[21] reported on heat generation and Joule heating effects on the Carreau fluid. The authors found that heat generation boosted temperature distribution of the fluid particles. [22] considered MHD flow fluid past an exponentially moving plate with radiation and varying heat source. They noticed that there is a decrease in the temperature field as the thermal relaxation influence is increasing. [23] examined the radiation effect on the conducting flow fluid influenced by pressure and magnetic field in nonlinear porous media with Soret and Dufour effects using symmetric Lie group. Their study revealed that the fluid molecular bonding force was influenced with rising radiation and magnetic field terms.[24], [25] investigated thermal radiation in the presence of nonlinear Boussinesq approximation for nanofluid. The model was numerically solved and indicated that the radiation term significantly impacted the heat transfer rate in the considered flow system. [26] also discussed heat generation and radiation impact on the conducting MHD Carreau nanofluid flow over an extended sheet. Temperature distribution was reportedly increased with rising heat generation and radiation terms. Hence, the essential of radiative heat and heat generation in a thermal species diffusion cannot be overly stressed as it has industrial significance. Therefore, managing thermal radiation and inner heat sink or production in a chemical reaction process is very critical, as reported by [27] and [28].

Furthermore, activation energy plays a critical part in the diffusion of binary chemical mixtures of energy and species transport phenomena as a minimum required energy for a chemical reaction to be produced from potential reactants. A quantitative and qualitative difference in the fluid heat transfer can be caused by species concentration difference with definite reaction activation energy, which is useful in water combinations, oil reservoir, and geothermal engineering [29]. Mass transfer and chemical reaction relation are complex as found in many manufacturing and consumption of reactant species. [30] analyzed the nanofluid chemical reaction of MHD flow in a vertical stratagem with buoyancy effects in the presence of activation energy. The species mixture activation energy was found to be directly proportional to the fluid concentration rate constant. [31] reflected on the declination of entropy generation for a nanomaterial radiative chemical binary reaction of MHD flow with activation energy over an extending surface. The activation energy caused a rising temperature field and thermal diffusivity of the species. [32] investigated covalent bonding of cross radiative nanofluid in axisymmetric with the effect of Arrhenius activation energy. From the computational outcome, the activation energy is found to have strongly influenced the concentration of the nanoparticle profile. Other reports on Arrhenius activation energy can be obtained from [33], [34], [35], and [36].

Due to its critical applications in the space technology, metallurgy, and pharmaceutical engineering industries, such as food processing technology, various hospital treatments, and polymer production, tremendous research has recently been conducted on the heat and mass transfer analysis of the flow over a stretching sheet. Furthermore, coupled heat and mass transfer problems involving homogeneous-heterogeneous reactions are important in a variety of engineering processes, thus they are receiving a lot of attention these days. The study of heat generation or absorption effect, in moving fluids is important in view of several physical problems such as fluid undergoing exothermic or endothermic chemical reactions. In many chemical engineering processes, chemical reactions take place between a foreign mass and the working fluid which moves due to the stretching of a surface. The order of the chemical reaction depends on several factors. One of the simplest chemical reactions is the first-order reaction in which the rate of reaction is directly proportional to the species concentration.

Inspired by this steady – state analysis of the convection problem, we feel that the inclusion of induced magnetic field and higher order chemical reaction would be interesting and useful for applications. Hence, we extend the work [37], [16], [38] and [39] to include thermal buoyancy and variable heat source. Thus, [39] become one of the special cases on this report. Hence, the applications and various suggestions from previous studies motivate the present investigation as it relates to technological improvement. It is our belief that the results of this research will

further provide deep insight into the effect of variable heat source and thermal buoyancy on Induced Magnetic Field

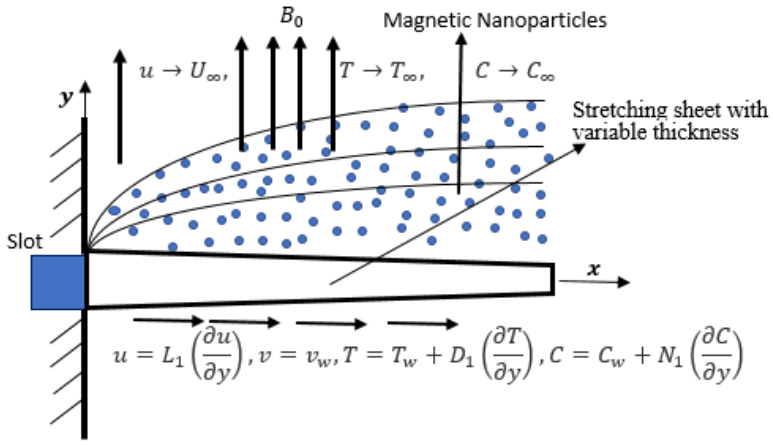

Figure 1: Schematic Diagram

Nano-Fluid Over a Stretching Wedge with Slip. We shall establish the agreement between our work and previous related articles especially [39]

2 Mathematical Modelling and Method of Solution

2.1 Mathematical/Problem formulation

Consider a coupled heat and mass transfer by hydro - magnetic flow of a continuously moving vertical permeable surface in the presence of surface suction, heat generation or absorption effects, transverse magnetic field effects and chemical reactions.

The flow is assumed unsteady, laminar and the surface is maintained at a uniform temperature and the concentration species, and is assumed to be infinitely long. It is also assumed that the applied transverse magnetic Reynolds number is significant so that the induced magnetic field is considered. The porous layer is homogeneous and isotropic and it is heated and salted from below. Furthermore, the effects like activation energy, exponential temperature-dependent heat source/sink, and variable thermal and molecular diffusivity are also considered during mathematical formulation of the problem. The flow is characterized by temperature dependent viscousity and conductivity. In addition, there is no applied electric field and all of the Hall effect, viscous dissipation and Joule heating are neglected, thermo - physical properties are assumed constant except the density in the buoyancy terms of the momentum equation. The fluid is assumed to be Newtonian, electrically conducting and its property variations due to temperature and induced magnetic field are limited to fluid density. The density variation is assumed to be negligible in the momentum equation (Boussinesq approximation). In addition, there is no applied electric field and all of the Hall effects and Joule heating are neglected. We assume that the induced magnetic field either also contribute to the fluid flow properties. Let the $x-$axis be taken along the direction of plate and y-axis normal to it. If u, v, T and $B_i, i = 1,2$ are the fluid x-component of velocity, $y-$component of velocity, temperature and induced magnetic respectively. Under the aforementioned assumptions and after utilizing the necessary boundary layer approximations the full equation of motion for a two-dimensional flow in Cartesian form regarding continuity, momentum, energy, and concentration are given as

$$\frac{\partial u}{\partial x} + \frac{\partial v}{\partial y} = 0, \tag{1}$$

$$\frac{\partial B_1}{\partial x} + \frac{\partial B_2}{\partial y} = 0, \tag{2}$$

$$\frac{\partial u}{\partial t} + u\frac{\partial u}{\partial x} + v\frac{\partial u}{\partial y} = u_e\frac{du_e}{dx} + \left(\frac{\mu_{nf}}{\rho_{nf}}\left(1+\frac{1}{\gamma}\right) + \frac{\nu_{nf}}{au_w}\left(\frac{\partial u}{\partial y}\right)\right)\frac{\partial^2 u}{\partial y^2} + \frac{g\beta}{\rho_{nf}}(T - T_\infty) + \frac{\mu_e}{4\pi\rho_{nf}}\left(B_1\frac{\partial B_1}{\partial x} + B_2\frac{\partial B_1}{\partial y} - B_e\frac{dB_e}{dx}\right) + \frac{g\beta_C}{\rho_{nf}}(C - C_\infty) \tag{3}$$

$$\frac{\partial B_1}{\partial t} + u\frac{\partial B_1}{\partial x} + v\frac{\partial B_1}{\partial y} = B_1\frac{\partial u}{\partial x} + B_2\frac{\partial u}{\partial y} + \mu_0\frac{\partial^2 B_1}{\partial y^2}, \tag{4}$$

$$\frac{\partial T}{\partial t}+u\frac{\partial T}{\partial x}+v\frac{\partial T}{\partial y}=\frac{k_{nf}}{\left(\rho c_p\right)_{nf}}\frac{\partial^2 T}{\partial y^2}+\frac{\mu_{nf}}{(c_p\rho)_{nf}}\left(1+\frac{1}{\gamma}\right)\left(\frac{\partial u}{\partial y}\right)^2+\frac{1}{\sigma(c_p\rho)_{nf}}\left(\frac{\partial B_1}{\partial y}\right)^2 + \frac{Dmk_T}{\left(\rho c_p\right)_{nf}C_w}\frac{\partial^2 C}{\partial y^2}+\frac{k_{nf}}{\left(\rho c_p\right)_{nf}}\frac{\partial q_r}{\partial y}+\frac{q'''}{\left(\rho c_p\right)_{hnf}} \quad (5)$$

$$\frac{\partial C}{\partial t}+u\frac{\partial C}{\partial x}+v\frac{\partial C}{\partial y}=\frac{D_m}{\rho_{n_f}}\frac{\partial^2 C}{\partial y^2}+\frac{D_T}{\rho_{nf}T_\infty}\frac{\partial^2 T}{\partial y^2} -\frac{k'\nu}{\tau\rho_{n_f}}\frac{\partial}{\partial y}\left((C-C_\infty)V_T\right)+k_r^2(C-C_\infty)^n \quad (6)$$

where μ_{nf} is density of hybrid nanofluid, T_∞ is the free stream temperature, σ_{hnf} is electrical conductivity, $B_0$is magnetic field, q_r is radiative heat flux, Q_0 is volumetric rate of heat source, k_{nf} is thermal conductivity of hybrid nanofluid and $\left(\rho c_p\right)_{hnf}$ is heat capacity of hybrid nanofluid. Where γ Casson fluid parameter, $\mu_e/4\pi\sigma_{nf}$ magnetic diffusivity μ_e is magnetic permeability, L is the characteristic length of the stretching surface, N is the velocity slip factor, B_0 is an estimation of the uniform magnetic field at the upstream infinity, $u_e(x)=ax$ is the velocity of the flow outside the boundary layer, $u_w(x)=cx$ is the velocity of the stretching sheet with c and a being the positive constants determining the strength of the stagnation point and stretching rate, and $B_e(x)=B_0(x/L)$ is the magnetic feld at the edge of the boundary layer. Also (B_x, B_y) are magnetic components in $(x\ , y)$ directions, respectively.

It is assumed that the radiation heat flux is to be presented in the form of an unidirectional flux in the y direction. Using the Roseland approximation for radiative heat transfer and the Roseland approximation for diffusion, the expression for the radiative heat flux q_r can be given as

$$q_r=\left(\frac{-4\sigma}{3k_s}\right)\left(\frac{\partial T^4}{\partial y}\right) \quad (6)$$

Here in Eq.(6), the parameters σ and k_s represent the Stefan Boltzmann constant and the Roseland mean absorption coefficient, respectively.

Now on assuming that the temperature differences within the fluid flow are sufficiently small, T^4 in Eq.(6) can be expressed as a linear function of T_∞ ' using the Taylor series expansion. The Taylor series expansion of T^4about T_∞ , after neglecting the higher order terms, takes the form

$$T^4\cong 4T_\infty^3T-3T_\infty^4=T_\infty^3(4T-3T_\infty) \quad (7)$$

Using equation (7) in (6), we have

$$q_r=\left(\frac{-16\sigma T_\infty^3}{3k_s}\right)\left(\frac{\partial T}{\partial y}\right) \quad (8)$$

The rate of heat generation is given as

$$q'''=\left(\frac{k_{nf}u_w(x)}{x\nu_{nf}}\right)\left[\frac{A^*(T_w-T_\infty)}{bx}u+Q_0(T-T_\infty)\right] \quad (6)$$

(A^*, Q_0) denoted the space and temperature dependent heat source/sink coefficient, respectively. Moreover, if $(A^*>0$ and $Q_0>0)$ correlates to internal heat generation, while when $(A^*<0$ and $Q_0<0)$ correlates to internal heat absorption.

Thus, on substituting (8) into (5), we have

$$\frac{\partial T}{\partial t}+u\frac{\partial T}{\partial x}+v\frac{\partial T}{\partial y}=\frac{k_{nf}}{\left(\rho c_p\right)_{nf}}\frac{\partial^2 T}{\partial y^2}+\frac{Dmk_T}{\left(\rho c_p\right)_{nf}C_w}\frac{\partial^2 C}{\partial y^2}+\frac{\mu_{nf}}{(c_p\rho)_{nf}}\left(1+\frac{1}{\gamma}\right)\left(\frac{\partial u}{\partial y}\right)^2 + \frac{1}{\sigma(c_p\rho)_{nf}}\left(\frac{\partial B_1}{\partial y}\right)^2-\frac{k_{nf}}{\left(\rho c_p\right)_{nf}}\frac{16\sigma T_\infty^3}{3k_s}\frac{\partial^2 T}{\partial y^2}+\left(\frac{k_{nf}u_w(x)}{x\nu_{nf}}\right)\left[\frac{A^*(T_w-T_\infty)}{cx}u+Q_0(T-T_\infty)\right] \quad (9)$$

The thermophoretic function is given by

$$V_T=-\frac{k'\mu_{n_f}}{T_r}\frac{\partial T}{\partial y} \quad (8)$$

and k' thermophoretic absorption constant and T_r reference temperature.

The boundary conditions at the plate surface and far into the cold fluid may be written as:

$$u=u_w(x)+N\left(1+\frac{1}{\gamma}\right)\frac{\partial u}{\partial y}, v=vw, \frac{\partial B_1}{\partial y}=B_2=0, -k_{nf}\frac{\partial T}{\partial y}=h(T_w-T), D_B\frac{\partial C}{\partial y}+\frac{D_T}{T_\infty}\frac{\partial T}{\partial y}=0 \text{ at } y=0 \quad (9)$$

$$u\to U_e, B_1\to B_e, T\to T_\infty, T\to T_\infty \text{ as } y\to\infty$$

where h is the plate heat transfer coefficient, T_w is the plate temperature of the hot fluid at the left surface of the plate and k_{hnf} is the thermal conductivity coefficient.

The surface temperature and concentration of the sheet is assumed to vary by both the sheet and time, in accordance with $T_w(x,t) = T_\infty + bx(1-\alpha t)^{-2}$ and $C_w(x,t) = C_\infty + bx(1-\alpha t)^{-2}$ respectively. The wall temperature and concentration $T_w(x,t)$, $C_w(x,t)$ increases (reduces), if b is positive (negative) and is in proportion to x. Moreover, the amount of temperature and concentration increase (reduce) along the sheet increases with time. Here $v_w(t) = -v_0/\sqrt{(1-\alpha t)}$ at is the velocity of suction $v_0 > 0$ or blowing $v_0 < 0$. The expression for $U_w(x,t), v_w(t), C_w(x,t), \lambda(t), \kappa_r(t)$ is valid for time $t < \alpha^{-1}$.

2.2 Rate of Heat and Mass Transfer at the wall

The quantities of engineering interest are the local Skin-Friction, Nusselt number and Sherwood number. These parameters characterize the wall heat and nano mass transfer rates. These parameters characterized the wall nano heat and mass transfer rates and are respectively define as follows:

The quantities Skin friction coefficient, Nusselt number and Sherwood number are denoted by c_f, Nu and Sh respectively and are define similar to [39] as follows:

$$c_f = \frac{\tau_w}{\rho_{nf} U_w^2}, Nu = \frac{x q_w}{k_{nf}(T_w - T_\infty)}, Sh_x = \frac{J_w}{D(C_w - C_\infty)} \tag{11}$$

where τ_w represents the skin friction along the surface, q_w the heat flux from the surface and

$$\tau_w = \left[\left(\mu_B + \frac{P_y}{\sqrt{2\pi_c}}\right)\frac{\partial u}{\partial y}\right]_{y=0}, q_w = \left[k_{nf}\left(1 - \frac{16\sigma T_\infty^3}{3k_s(\rho c_p)_{nf}}\right)\frac{\partial T}{\partial y}\right]_{y=0}, J_w = -D\frac{\partial C}{\partial y}\Big|_{y=0} \tag{13}$$

where U_w, q_w and J_w, represents the wall shear stress, heat transfer and mass transfer respectively.

3. Method of Solution

3.1. Similarity Transformation

To seek for solution, we sought for a stream function $\psi(x,y,t)$ which must identically satisfied continuity equations, such that the stream function $\psi_{u,B}$ corresponding to velocity and magnetic field respectively, satisfies the continuity equation (1) and (2) automatically with

$$u = \frac{\partial \psi_u}{\partial y} \text{ and } v = -\frac{\partial \psi_u}{\partial x}, \qquad u = \frac{\partial \psi_B}{\partial y} \text{ and } v = -\frac{\partial \psi_B}{\partial x} \tag{12}$$

A similarity solution of Equations (1) – (4) and (10) and (11) are obtained by defining an independent variable η and dependent variables f and g in terms of the stream function ψ as

$$\eta = y\sqrt{\frac{U_w}{\nu x(1-\alpha t)}}, \psi_u = \sqrt{\frac{\nu_{nf} x U_w}{1-\alpha t}} f(\eta), \qquad \psi_B = \sqrt{\frac{\nu_{nf} x B_e}{1-\alpha t}} g(\eta) \tag{13}$$

The dimensionless temperature and concentration transformation are given as

$$\theta(\eta) = \frac{T - T_\infty}{T_w - T_\infty}, \qquad \phi(\eta) = \frac{C - C_\infty}{C_w - C_\infty}. \tag{14}$$

But U_w and B_e are defined respectively as

$$u_w(x) = \frac{cx}{(1-\alpha t)} \text{ and } B_e(x) = B_0\left(\frac{x}{L(1-\alpha t)}\right) \tag{15}$$

Thus with (15), equation (13) implies

$$\eta = y\sqrt{\frac{c}{\nu_{nf}(1-\alpha t)}}, \psi_u = x\sqrt{\frac{\nu_{nf} c}{1-\alpha t}} f(\eta), \qquad \psi_B = x\sqrt{\frac{\nu_{nf} B_0}{L(1-\alpha t)}} g(\eta) \tag{16}$$

Hence, we can obtain the following identities conveniently;

$$\begin{gathered} u = \frac{cx}{1-\alpha t} f'(\eta), v = -\frac{\sqrt{\nu_{nf} c}}{1-\alpha t} f(\eta), \\ B_1 = x\sqrt{\frac{cB_0}{L(1-\alpha t)}} g'(\eta) \text{ and } B_2 = -\sqrt{\frac{\nu_{nf} B_0}{L}} g(\eta) \end{gathered} \tag{17}$$

Where

$$T_w(x,t) = T_\infty + bx(1-\alpha t)^{-2}, C_w(x,t) = C_\infty + bx(1-\alpha t)^{-2}$$

Using equations (14) - (19), dimensionless form of (3), (4) and (9) are obtained as

$$\left(\left(1+\frac{1}{\gamma}\right)+\delta_1\left(\frac{\partial^2 f(\eta)}{\partial\eta^2}\right)^2\right)\frac{\partial^3 f(\eta)}{\partial\eta^3}-\frac{\kappa}{A_2}\left(\left(\frac{\partial g(\eta)}{\partial\eta}\right)^2+g(\eta)\frac{\partial^2 g(\eta)}{\partial\eta^2}-1\right)+\lambda^2$$
$$-A_1\left(\left(\frac{\partial f(\eta)}{\partial\eta}\right)^2-f(\eta)\frac{\partial^2 f(\eta)}{\partial\eta^2}+\alpha_1\left(\frac{\partial f(\eta)}{\partial\eta}+\frac{\eta}{2}\frac{\partial^2 f(\eta)}{\partial\eta^2}\right)\right)+Gr\big(\theta(\eta)+\mathrm{N}\phi(\eta)\big)=0 \quad (20)$$

$$\frac{\partial^3 g(\eta)}{\partial\eta^3}+\frac{A_5}{\Omega}\left(f(\eta)\frac{\partial^2 g(\eta)}{\partial\eta^2}-g(\eta)\frac{\partial^2 f(\eta)}{\partial\eta^2}\right)-\frac{\alpha_1}{2}\left(\frac{\partial g(\eta)}{\partial\eta}+\eta\frac{\partial^2 g(\eta)}{\partial\eta^2}\right)=0 \quad (21)$$

$$\left(A_4-\frac{4R_d}{3}\right)\frac{\partial^2\theta(\eta)}{\partial\eta^2}+\mathrm{Pr}Ec\left(1+\frac{1}{\gamma}\right)\left(\frac{\partial^2 f(\eta)}{\partial\eta^2}\right)^2-A_3\,\mathrm{Pr}\left(\alpha_1\frac{\eta}{2}-f(\eta)\right)\frac{\partial\theta(\eta)}{\partial\eta}$$
$$+A_4\alpha_0\left(\frac{\partial^2 g(\eta)}{\partial\eta^2}\right)^2+Du\frac{\partial^2\phi(\eta)}{\partial\eta^2}+A_4\left(A^*\frac{\partial f(\eta)}{\partial\eta}+B^*\theta(\eta)\right)=0 \quad (22)$$

$$\frac{\partial^2\phi(\eta)}{\partial\eta^2}+Sr\frac{\partial^2\theta(\eta)}{\partial\eta^2}-Le\beta\frac{\partial}{\partial\eta}\left(\phi(\eta)\frac{\partial\theta(\eta)}{\partial\eta}\right)-Le\alpha_1\left(\frac{\eta}{2}-f(\eta)\right)\frac{\partial\phi(\eta)}{\partial\eta}+\delta\phi(\eta)^n=0 \quad (23)$$

Dimensionless form of boundary conditions (10) becomes

$$\left.\begin{aligned} f'(0)=1+V\left(1+\frac{1}{\gamma}\right)\frac{\partial^2 f(0)}{\partial\eta^2}, f(0)=S, g''(0)=0, g(0)=0 \\ Bi\frac{\partial\theta(0)}{\partial y}=-\big(1-\theta(0)\big), \omega\frac{\partial\phi(0)}{\partial y}=-(1-r\theta(0)) \\ \frac{\partial f(\eta)}{\partial\eta}\to\lambda, \frac{\partial g(\eta)}{\partial\eta}\to 1, \theta(\eta)\to 0, \phi(\eta)\to 0 \quad \text{as } \eta\to\infty \end{aligned}\right\}, \quad (24)$$

The emerging dimensionless flow governing parameters are defined by

$$\alpha_1=\frac{\alpha}{c}, Pr=\frac{(\mu c_p)_f}{k_f}, R=\frac{4\sigma T_\infty^3}{k_s}, \alpha_0=\frac{B_e^2}{(T_w-T_\infty)B_0^2\kappa_f\sigma}, S=-\frac{v_0}{\sqrt{\nu_{nf}c}}, \lambda=\frac{a}{c}, Pm=\sigma\nu_f\mu_f,$$
$$Le=\frac{\mu_f}{Dm}, Pr=\frac{\mu_f c_{p_f}}{k_f}, \delta_1=\frac{(1-\alpha t)k_r^2(C_w-C_\infty)^{n-1}}{c\rho_{nf}}, Ec=\frac{c^2x^2}{(c_p)_{nf}(T_w-T_\infty)}, \frac{\kappa_f}{A_2}=\frac{(1-\alpha t)B_0\mu_e}{4cL\pi\rho_f}$$
$$\frac{1}{Le}=\frac{D_m}{\mu_f}, \frac{1}{Pr}=\frac{\kappa_f}{\mu_f c_{p_f}}, Gr=\frac{g\beta_T(T_w-T_\infty)}{\rho_{nf}c^2x}, Sr=\frac{D_T(T_w-T_\infty)}{T_\infty D_m(C_w-C_\infty)}, Du=\frac{D_m(C_w-C_\infty)}{C_w(T_w-T_\infty)},$$
$$\beta=\frac{(T_w-T_\infty)k_f}{T_r}, \mu_0=\frac{1}{4\pi\mu_e\sigma_f}, A_5=\frac{\sigma_{nf}}{\sigma_f}, N=\frac{\beta c(C_w-C_\infty)}{\beta t(T_w-T_\infty)}, r=\frac{T_w-T_\infty}{T_\infty}$$

3.2 Non-Dimensional Skin-Friction and wall Heat Transfer

In non-dimensional form, the rate of heat transfer at the wall is computed from Fourier's law which represent the skin friction along the surface and the Nusselt number represent the heat transfer at the wall. These parameters characterized the wall nano heat and mass transfer rates and are respectively define as follows:

$$c_f=\frac{\tau_w}{\rho_{nf}U_w^2}=\frac{\mu_{nf}}{\rho_{nf}U_w^2}\left[\left(1+\frac{1}{\gamma}\right)\frac{\partial u}{\partial y}+\frac{\nu_{nf}\gamma}{u_w\gamma}\left(\frac{\partial u}{\partial y}\right)^3\right]_{y=0}=\frac{1}{\sqrt{Re}}\left[\left(1+\frac{1}{\gamma}\right)\frac{\partial f'(\eta)}{\partial\eta}+\frac{A_1S}{\gamma}\left(\frac{\partial f'(\eta)}{\partial\eta}\right)^3\right]_{y=0}$$
$$\Rightarrow c_f(Re_x)^{1/2}=\left[\left[\left(1+\frac{1}{\gamma}\right)\frac{\partial^2 f(\eta)}{\partial\eta^2}+\frac{A_1S}{\gamma}\left(\frac{\partial^2 f(\eta)}{\partial\eta^2}\right)^3\right]\right]_{\eta=0} \quad (22)$$

$$Nu=\frac{xq_w}{k_{nf}(T_w-T_\infty)}=-\sqrt{Re}\left[\left(A_4-\frac{4}{3}Rd\right)\frac{\partial\theta(\eta)}{\partial\eta}\right]_{y=0}\Rightarrow Nu(Re_x)^{-1/2}=-\left(A_4-\frac{4}{3}Rd\right)\left[\frac{\partial\theta(\eta)}{\partial\eta}\right]_{\eta=0} \quad (23)$$

$$Sh_x=\frac{J_w}{D(C_w-C_\infty)}=-\sqrt{Re}\left[\frac{\partial\phi(\eta)}{\partial\eta}\right]_{y=0}\Rightarrow Sh(Re_x)^{-1/2}=-\left.\frac{\partial\phi(\eta)}{\partial\eta}\right|_{\eta=0}. \quad (24)$$

Where the local Reynolds number (Re_x) is define as

$$Re_x = xu_w/\nu_f = \frac{cx^2}{\nu_f(1-\alpha t)}$$

3.3 Solution by Homotopy analysis method

The HAM is an analytical method which involves obtaining a set of base functions for the representation of the problem at hand. We chose our base functions as $f(\eta), g(\eta)$, and $\theta(\eta)$ because at infinity, the boundary layer flows are decaying exponentially:

$$f(\eta) = a_{0,0}^* + \sum_{k=0}^{\infty}\sum_{n=1}^{\infty} a_{k,n}^* \eta^k e^{-n\eta}$$
$$g(\eta) = b_{0,0}^* + \sum_{k=0}^{\infty}\sum_{n=1}^{\infty} b_{k,n}^* \eta^k e^{-n\eta}$$
$$f(\eta) = c_{0,0}^* + \sum_{k=0}^{\infty}\sum_{n=1}^{\infty} c_{k,n}^* \eta^k e^{-n\eta}$$

where the $a_{i,k}^*, b_{i,k}^*$ and $c_{i,k}^*$ are constants.

The approximation of $f, g,$ and θ must obey the above equations which is called the rule of solution for the them.

Following the boundary conditions and the rule of the solution, we have the initial approximations as:

$$f_0(\eta) = 1 + \frac{1 - exp(-\eta)}{1 + \lambda_1\left(1 + \frac{1}{\gamma}\right)}, g_0(\eta) = exp(-\eta), \theta_0(\eta) = \frac{\beta i}{N_3}(e^{-\eta} - 1)$$

Also, the auxiliary linear operators are given as:

$$L_f(f) = \frac{d^3}{d\eta^3}f - \frac{d}{d\eta}f, L_g(g) = \frac{d^3}{d\eta^3}g - \frac{d}{d\eta}g, L_\theta(\theta) = \frac{d^3}{d\eta^3}\theta - \theta$$

Satisfying

$$L_f(c_4e^{-\eta} + c_3e^{-\eta} + c_2\eta + c_1) = 0, L_g(c_7e^{-\eta} + c_6e^{\eta} + c_5) = 0, L_\theta(c_8e^{\eta} + c_9e^{-\eta}) = 0$$

where the c_s are constants.

If the embedding and non-zero parameters are given as $0 \le p \le 1$, and $(\hbar_f, \hbar_g, \hbar_\theta)$ respectively, then the deformation problems (of zeroth order) are:

$$(1-p)\big(f(\eta,p) - f_0(\eta)\big)L_f = N_f(f,g,\theta)p\hbar_f$$
$$(1-p)\big(g(\eta,p) - g_0(\eta)\big)L_g = N_g(f,g,\theta)p\hbar_g$$
$$(1-p)\big(\theta(\eta,p) - \theta_0(\eta)\big)L_\theta = N_\theta(f,g,\theta)p\hbar_\theta$$

The corresponding boundary equations are:

$$f'(0,p) = 1 + \lambda_1\left(1 + \frac{1}{\gamma}\right)f''(0,p), f(0,p) = S, f'(\infty,p) = A$$
$$g''(0,p) = 0, g(0,p) = 0, g'(\infty,p) = 1$$
$$\omega\theta'(0,p) = -(1-\theta), \theta(\infty,p) = 0$$

as p changes from 0 to 1, $f_0(\eta), g_0(\eta)$ and $\theta_0(\eta)$ approach $f(\eta,p), g(\eta,p)$ and $\theta(\eta,p)$ respectively.

By Taylor's series expansion,

$$f(\eta;\, p) = f_0(0) + \sum_{n=1}^{\infty} f_m(\eta)p^n, g(\eta;\, p) = g_0(0) + \sum_{n=1}^{\infty} g_m(\eta)p^n$$
$$\theta(\eta;\, p) = \theta_0(0) + \sum_{n=1}^{\infty} \theta_m(\eta)p^n, \phi(\eta;\, p) = \phi_0(0) + \sum_{n=1}^{\infty} \phi_m(\eta)p^n$$

where

$$f_m(\eta;\, p) = \frac{1}{k!}\frac{\partial^m}{\partial\eta^m}f(\eta;\, p), g_m(\eta;\, p) = \frac{1}{k!}\frac{\partial^m}{\partial\eta^m}g(\eta;\, p),$$
$$\theta_m(\eta;\, p) = \frac{1}{k!}\frac{\partial^m}{\partial\eta^m}\theta(\eta;\, p), \phi_m(\eta;\, p) = \frac{1}{k!}\frac{\partial^m}{\partial\eta^m}\phi(\eta;\, p)$$

At $p = 1$ the series equations 1 and 2 converge if the following parameters: initial guesses, auxiliary linear operators, and the auxiliary are chosen appropriately. Hence,

$$f(\eta) = f_0(\eta) + \sum_{n=1}^{\infty} f_m(\eta), g(\eta) = g_0(\eta) + \sum_{n=1}^{\infty} g_m(\eta)$$

$$\theta(\eta) = \theta_0(\eta) + \sum_{n=1}^{\infty} \theta_m(\eta), \phi(\eta) = \phi_0(\eta) + \sum_{n=1}^{\infty} \phi_m(\eta)$$

The *dth - order* deformation problems are:

$$L_f(f_d - \chi_d f_{d-1} = \hbar_f R_d^f(\eta), L_g(g_d - \chi_d g_{d-1} = \hbar_g R_d^g(\eta)$$
$$L_\theta(\theta_d - \chi_d \theta_{d-1} = \hbar_\theta R_d^\theta(\eta), L_\Phi(\Phi_d - \chi_d \Phi_{d-1} = \hbar_\theta R_d^\Phi(\eta)$$

Table 1: Skin-friction, Sherwood and Nusselt number for various values of parameter

	$f''(0)$	$\phi'(0)$	$\theta'(0)$		$f''(0)$	$\phi'(0)$	$\theta'(0)$
$\alpha_1 = 0.01$	-0.995111	0.161297	-6.414047	$\lambda = 0.0$	-1.186811	0.112066	-6.039250
$\alpha_1 = 0.05$	-1.006193	0.167257	-6.395599	$\lambda = 0.2$	-1.017993	0.186360	-6.483918
$\alpha_1 = 0.1$	-1.019516	0.175038	-6.372722	$\lambda = 0.4$	-0.788811	0.247884	-6.892394
$\alpha_1 = 0.2$	-1.044417	0.191765	-6.327371	$\lambda = 1.2$	0.675767	0.169660	-7.218612
$Le = 0.5$	-0.941740	2.242965	-7.512009	$\kappa = 0.0$	-1.002309	0.180959	-6.451934
$Le = 1.0$	-0.989628	1.119776	-6.920784	$\kappa = 1.0$	-1.098695	0.174696	-6.390421
$Le = 2.0$	-1.014173	0.185243	-6.466521	$\kappa = 3.0$	-1.246742	0.159776	-6.269489
$Le = 3.0$	-1.038390	-1.494091	-5.668529	$\kappa = 6.0$	-1.393169	0.142991	-6.143704
$Sr = 0.0$	-1.032775	-1.831770	-5.517776	$N = 0.1$	-1.055867	0.183322	-6.456387
$Sr = 0.2$	-1.025406	-0.902069	-5.961982	$N = 0.6$	-0.992856	0.188191	-6.501308
$Sr = 0.4$	-1.017993	0.186360	-6.483918	$N = 1.6$	-0.868387	0.195157	-6.577461
$Sr = 0.5$	-1.014269	0.802956	-6.780412	$N = 3.2$	-0.672714	0.199534	-6.666042
$\beta = 0.1$	-1.017993	0.186360	-6.483918	$Gr = 0.0$	-1.093447	0.180355	-6.429699
$\beta = 0.2$	-1.021359	-0.361485	-6.221075	$Gr = 0.5$	-0.999200	0.187674	-6.496576
$\beta = 0.3$	-1.024374	-0.821238	-6.000834	$Gr = 1.0$	-0.905503	0.193169	-6.554776
$\beta = 0.4$	-1.027102	-1.215880	-5.812025	$Gr = 2.0$	-0.718394	0.199070	-6.647469
$Rd = 0.0$	-1.011443	0.127714	-6.232691	$Ec = 0.0$	-1.026780	0.413585	-7.417163
$Rd = 0.05$	-1.011692	0.153708	-6.338058	$Ec = 0.5$	-1.017993	0.186360	-6.483918
$Rd = 0.10$	-1.011933	0.180611	-6.447290	$Ec = 1.0$	-1.009184	-0.042451	-5.558240
$Rd = 0.25$	-1.012605	0.267284	-6.800451	$Ec = 1.5$	-1.000352	-0.272838	-4.640141
$n = 0.0$	-0.976461	0.720419	-6.750778	$\alpha_0 = 0.0$	-1.020460	0.209554	-6.575060
$n = 1.0$	-1.011933	0.180611	-6.447290	$\alpha_0 = 0.1$	-1.017993	0.186360	-6.483918
$n = 2.0$	-1.013320	0.136662	-6.426205	$\alpha_0 = 0.2$	-1.015525	0.163089	-6.392593
$n = 3.0$	-1.013654	0.121214	-6.418922	$\alpha_0 = 0.5$	-1.008108	0.092808	-6.117509
$Du = 0.0$	-1.044003	0.103155	-6.259825	$\varphi = 0.0$	-1.217147	0.339391	-7.002714
$Du = 1.0$	-1.039772	0.126203	-6.358817	$\varphi = 0.4$	-0.457625	-0.420157	-4.330721
$Du = 2.0$	-1.035486	0.152852	-6.472317	$\varphi = 0.6$	-0.129797	-0.925658	-2.545722
$Du = 2.5$	-1.033318	0.167761	-6.535486	$\varphi = 0.8$	0.280587	-1.549161	-0.356785
$\Omega = 0.4$	-1.011966	0.180594	-6.447212	$\delta = -0.6$	-1.024791	-0.154981	-6.321343
$\Omega = 0.8$	-1.011556	0.180791	-6.448107	$\delta = -0.2$	-1.021801	0.001698	-6.395878
$\Omega = 1.4$	-1.010710	0.181177	-6.449885	$\delta = 0.2$	-1.017993	0.186360	-6.483918
$\Omega = 2.4$	-1.008925	0.182051	-6.454040	$\delta = 0.6$	-1.012879	0.413779	-6.592661

Table 2: Effect of Slip condition on rate of heat transfer at the wall

	$f''(\eta)$	$\phi'(\eta)$	$\theta'(\eta)$		$f''(\eta)$	$\phi'(\eta)$	$\theta'(\eta)$
$V = 0.0$	-1.191737	0.088101	-6.175432	$Bi = -0.5$	-1.033394	-1.906548	1.648379
$V = 0.2$	-0.889001	0.252905	-6.685767	$Bi = -0.1$	-1.050398	-4.320467	9.789199
$V = 0.4$	-0.709943	0.336187	-6.926648	$Bi = 0.1$	-1.017993	0.186360	-6.483918
$V = 0.8$	-0.506875	0.417743	-7.142987	$Bi = 0.3$	-1.027228	-1.057945	-1.516120
$S = 0.0$	-0.663751	-0.250730	-0.924433	$\varphi = 0.0$	-1.217147	0.339391	-7.002714
$S = 0.4$	-0.709054	0.347763	-3.967396	$\varphi = 0.4$	-0.457625	-0.420157	-4.330721
$S = 0.8$	-0.808640	0.426594	-5.348031	$\varphi = 0.6$	-0.129797	-0.925658	-2.545722
$S = 1.2$	-0.923874	0.317679	-6.094311	$\varphi = 0.8$	0.280587	-1.549161	-0.356785

With the conditions:

$$f_d'(\eta,0)=1+V\left(1+\frac{1}{\gamma}\right)f_d''(0), f_d(\eta)=S, f_d'(\infty)=\lambda, g_d''(\eta)=0, g_d(\eta)=1, g_d'(\infty)$$

$$Bi\frac{\partial\theta_d(\eta)}{\partial\eta,}=-\left(1-\theta_d(\eta)\right), \theta_d(\infty)=0, \omega\frac{\partial\phi_d(\eta,0)}{\partial\eta,}=-\left(1-r\theta_d(\eta,0)\right), \phi_d(\infty)=0$$

where

$$R_d^f(\eta)=\left(\left(1+\frac{1}{\gamma}\right)+\delta\sum_{k=1}^{d=1}f_{d-1-k}''\right)\sum_{k=1}^{d=1}f_{d-1}'''-\frac{\kappa}{A_2}\left(\sum_{k=1}^{d=1}g_{d-1-k}'g_j'+\sum_{k=1}^{d=1}g_{d-1-k}'g_k''-1\right)+\lambda^2$$
$$-A_1\left(\sum_{k=1}^{d=1}f_{d-1-k}''f_k-\sum_{k=1}^{d=1}f_{d-1-k}'f_k'+\alpha_1\left(\sum_{k=1}^{d=1}f_{d-1-k}'+\frac{\eta}{2}\sum_{k=1}^{d=1}f_{d-1-k}''\right)\right)+Gr(\theta_{d-1}+\mathrm{N}\phi_d)$$

$$R_d^g(\eta)=\sum_{k=1}^{d=1}g_{d-1-k}''+\frac{A_5}{Pm}\left(\sum_{k=1}^{d=1}f_{d-}g_{d-1-k}''-\sum_{k=1}^{d=1}g_{d-}f_{d-1-k}''\right)-\frac{\alpha_1}{2}\left(\sum_{k=1}^{d=1}g'_{\ d}+\eta\sum_{k=1}^{d=1}g_{d-1-k}''\right)$$

$$R_d^\theta=\left(A_4-\frac{4R_d}{3}\right)\sum_{k=1}^{d=1}\theta_{d-1-k}''+\mathrm{Pr}Ec\left(1+\frac{1}{\gamma}\right)\sum_{k=1}^{d=1}\theta_{d-1-k}''\theta_k''-A_3\,\mathrm{Pr}\left(\alpha_1\frac{\eta}{2}-\sum_{k=1}^{d=1}f_k\right)\sum_{k=1}^{d=1}\theta_k'$$
$$+A_4\alpha_0\sum_{k=1}^{d=1}g_{d-1-k}''g_k''+Du\sum_{k=1}^{d=1}\phi_{d-1-k}''\phi_k''+A_4\left(A^*\sum_{k=1}^{d=1}f_{d-1-k}'+B^*\theta_d\right)$$

$$R_d^\phi=\sum_{k=1}^{d=1}\phi_{d-1-k}''\phi_k''+Sr\sum_{k=1}^{d=1}\theta_{d-1-k}''\theta_k''-\beta\sum_{k-1}^{d-1}\left(\phi_d\sum_{k=1}^{d=1}\theta_{d-1-k}'\right)-\alpha_1\left(\frac{\eta}{2}-\sum_{k=1}^{d=1}f_k\right)\sum_{k=1}^{d=1}\phi_{d-1-k}'+\delta_1\phi(\eta)^n$$

Where $\chi=0$ when $d\leq 1$ *and* $\chi=1$ when $d>1$

Hence, the general solutions are:

$$f_d(\eta)=f_d(\eta)'+c_1+c_2\eta+c_3\eta^2+c_4\eta^3$$
$$g_d(\eta)=g_d(\eta)'+c_5+c_6e^{\eta}+c_7e^{-\eta}$$
$$\theta_d(\eta)=\theta_d(\eta)'+c_8e^{\eta}+c_9e^{-\eta}$$

Here, $f_d(\eta)', g_d(\eta)'$ and $\theta_d(\eta)'$ are the particular solution, while $c's$ are constants which were determined by the boundary conditions.

Lastly, the equations are coded and executed in a symbolic system MAPLE 2021 package.

Table 3: Computed initial data and skin-friction, Sherwood and Nusselt number for space heat generation or absorption

Computed Initial data							
Space heat source	$f'(0)$	$f''(0)$	$g'(0)$	$\phi(0)$	$\theta(0)$	$\phi'(0)$	$\theta'(0)$
$(A^*,B^*)=(-3,-9)$	0.9	-1.0	1.2	1.0	0.2544	0.4318	-7.4562
$(A^*,B^*)=(-1,-3)$	0.9	-1.0	1.2	1.0	0.3108	0.2916	-6.8924
$(A^*,B^*)=(0.7,0.2)$	0.9	-1.0	1.2	1.0	0.3787	0.1218	-6.2131
$(A^*,B^*)=(2,2)$	0.9	-1.0	1.2	1.0	0.4392	-0.0306	-5.6083

4. Discussion of Results

We have used the Homotopy Analysis Method (HAM) that uses the homotopy parameter that split nonlinear system into an infinite set of linear systems which are solved analytically, while the continuation methods require solving a discrete linear system as the homotopy parameter is varied to solve the nonlinear system. The procedure that generates the result numerically and graphed is codded in Wolfram mathematical language. The result of the computation are displayed using figures, Figure 2-25 and Table 1-3. The discussion of both the graphs and the tables are set out below.

4.1 Validity of Results

In order to assess the accuracy of the numerical method, we have compared the present results of $f''(0)$ for different values of α with $\beta=0$ and $\gamma\to\infty$ in the absence of the energy equation versus the previously published data of Mahapatra and Gupta [38], Ishak et al. [39], Ali et al. [26] and Mohamed and Ali [39]. The comparison is listed in Table 1 and found in excellent agreement.

4.2 Velocity: The velocity distribution is examined considering the impact of stretching velocity λ, buoyancy ratio, Grashof number N, slip velocity V, suction velocity S and nano-fluid parameter φ. We display in Figure 2 the impact of stretching velocity on velocity distribution, from this figure, it could be seen that velocity increases as stretching velocity increases. Also, at a higher stretching velocity, we observed that velocity close to the surface is higher that the velocity at the surface. The velocity boundary layer was also seen to increase with increase in stretching velocity. While both buoyancy ratio and Grashof (thermal) increases the velocity distributions as displayed in Fig 3 and 4. The effect of velocity slip and suction velocity are shown in Figure 5 and 6 respectively. From the figures, we observed that increase in both parameters, velocity slip and suction velocity decreases the velocity boundary. Figure 7 displayed the impact of nano-fluid parameter on the velocity distribution. The figure indicate that velocity is enhanced with increases in nano-fluid parameter.

4.3 Induced Magnetic Field: Magnetic induced of the flow is described using figures 8-13 with the of flow governing parameters; unsteadiness parameter α_1, nano-fluid parameter φ, magnetic Prandtl number Ω, stretching velocity λ, magnetic inductance κ and velocity slip V. Figure 8 indicates unsteadiness parameter declines the induced magnetic field as unsteadiness parameter increases, the induced magnetic boundary layer reduces while nanofluid parameter enhances induced magnetics as shown in Figure9. Figure 10-13 shows the enhancement effects of stretching velocity, magnetic inductance and velocity slip on induced magnetic field. It was observed that increase in those parameters declines the induced magnetic field.

4.4 Temperature: The impact of Eckert number, magnetic parameter α_0, Dufort number, stretching velocity, nanofluid parameter, Lewis number on temperature distribution were explained through figures 14-18. These graphical illustrations are just in two folds viz: Eckert number, magnetic parameter, Dufort number and nanofluid parameter were observed to enhances the temperature distributions. Further, close to the surface of flow, temperature dropped rapidly and the approaches zero asymptotically as displayed in Figure 14-16 and 18 respectively whereas, stretching velocity decline the temperature distributions.

4.4 Concentration: We displayed the effect of Lewis number on concentration of the flow field in Figure 19, from this figure we observed that concentration boundary layer decline as Lewis number increases. So also, we discovered that concentration flux at the surface depends on the values of Lewis number. Soret number was discovered to enhances concentration of the flow field as displayed in Figure 20. In Figure 21, stretching velocity declines the concentration and we deduced from the figure that the profile is independent of the value of stretching velocity. While suction velocity and concentration slip bring about decline in concentration of the flow field as displayed in Figure 22 and Figure 24. This observation is practically correct as suction or slip have the tendencies of reducing the chemical species in the flow field leaving behind less concentration. Figure 23 displayed the effect of convective surface temperature, from where we discovered that when heat moves from solid surface to fluid ($Bi < 0$) the temperature of the fluid flow increases whereas, when heat moves from fluid to the solid surface ($Bi > 0$), the bulk temperature of the fluid declines. The reactivity parameter of the chemical species was seen to increase the species concentration for the case of generative chemical reaction ($\delta > 0$) and decline the concentration boundary layer for destructive reaction ($\delta < 0$) as displayed in Figure 25.

4.5 Rate of heat and mass transfer at the wall: The flow rate at the wall in terms of skin friction $f''(0)$, heat flux $\theta'(0)$ and concentration transfer at the wall $\phi'(0)$ is displayed in Table 1. The effect of the flow governing parameters were explained using the data contained in the table. From the table, we discovered that unsteadiness parameter, Lewis number, thermophoretic parameter β, radiation, reaction order, Dufort number Du and magnetic inductance κ, decline skin-friction of the flow whereas, Soret number, Magnetic Prandtl number, stretching velocity, buoyancy ratio, Grashof number, Eckert number, magnetic inductance, nanofluid parameter, and reactivity parameter enhances the skin-friction. In this same vein, the effect of all these parameters on Sherwood and Nusselt number are displayed in the table and self-explained. The effect of Slip condition on rate of heat and mass transfer at the wall is displayed in Table 2. From this table, we discovered that slip velocity increases skin-friction and Nusselt number and decline Sherwood number of the flow field. Increases in Suction velocity decreases skin-friction and Nusselt number, while increases in Nanofluid parameter increases the skin friction and Nusselt number and, decline the Sherwood number. We also compute the initial data for the system of equations for specifi space heat source. The corresponding initial data were displayed in Table 3.

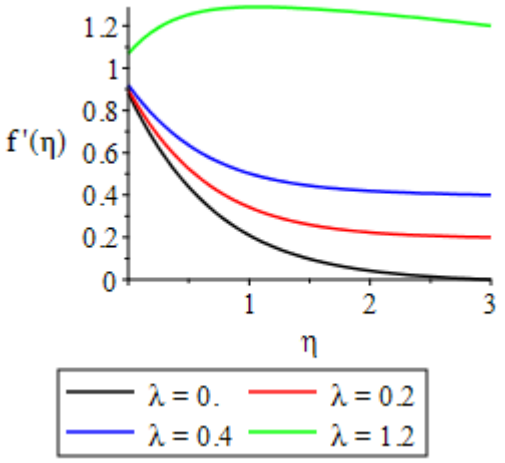

Figure 2: Effect of stretching velocity on velocity distribution

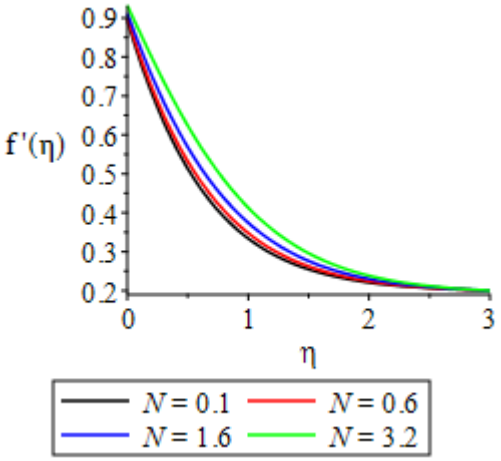

Figure 3: Effect of buoyancy ratio on velocity distribution

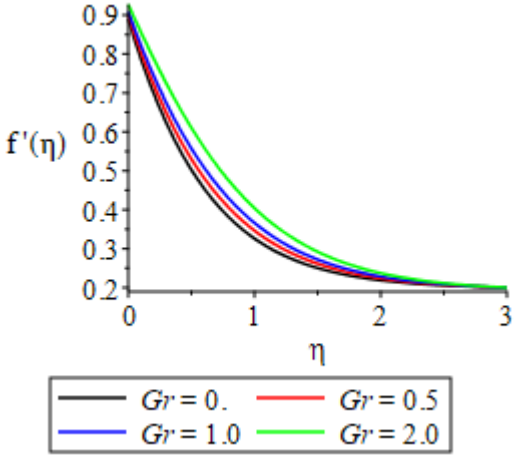

Figure 4: Effect of thermal Grashof number on velocity distribution

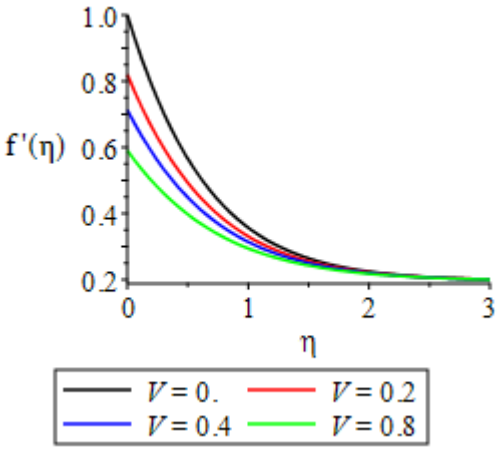

Figure 5: Effect of velocity slip on velocity distribution

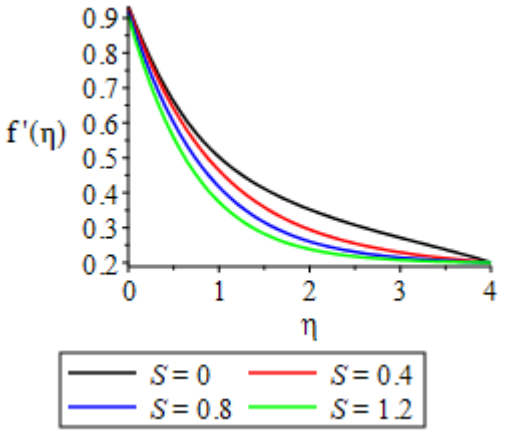

Figure 6: Effect of suction velocity on velocity distribution

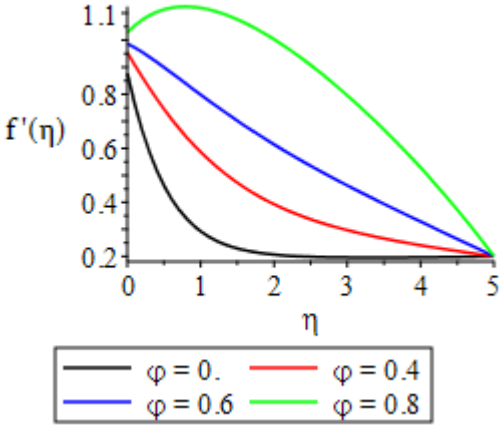

Figure 7: Effect of nano parameter on velocity distribution

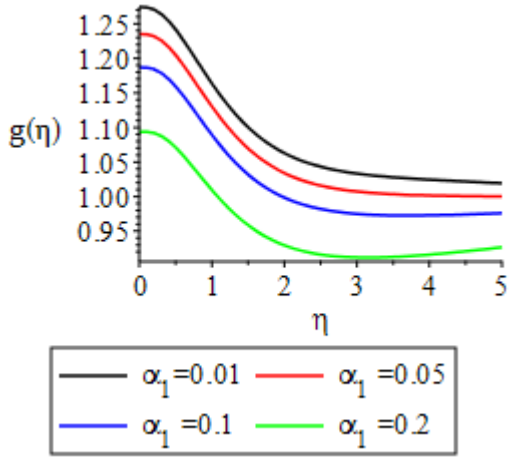

Figure 8: Effect of unsteadiness parameter on induced magnetic field

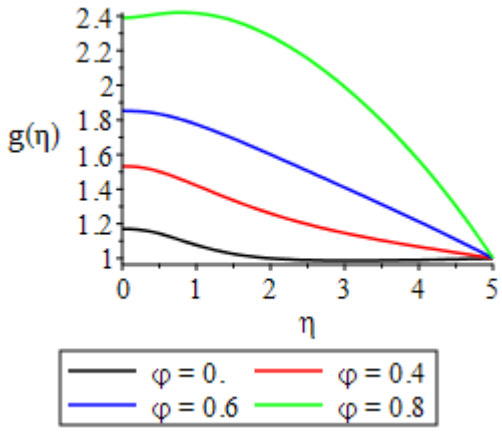

Figure 9: Effect of Nanofluid parameter on induced magnetic field

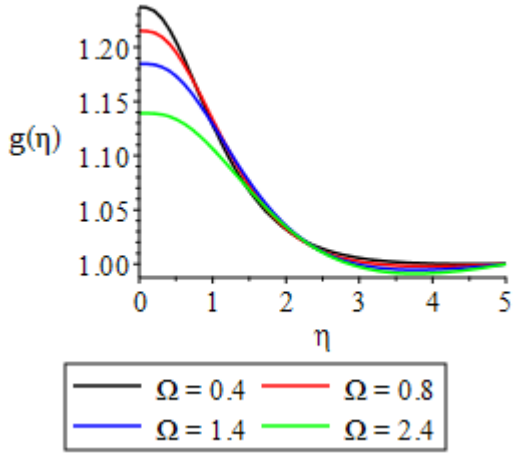

Figure 10: Effect of magnetic Prandtl number on induced magnetic field

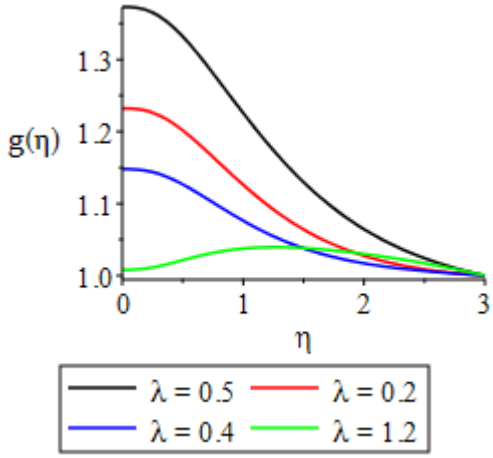

Figure 11: Effect of stretching velocity on induced magnetic field

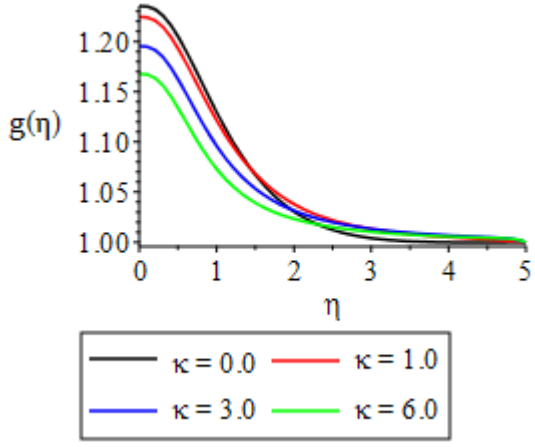

Figure 12: Effect of magnetic inductance on induced magnetic field

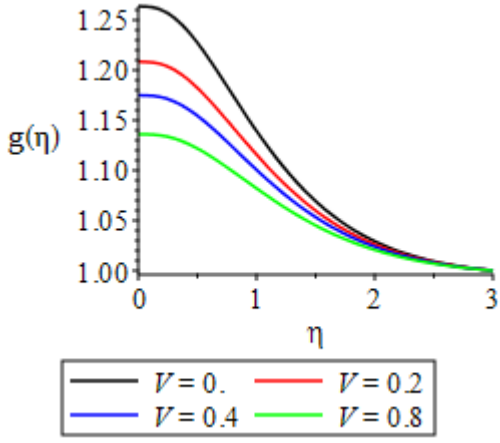

Figure 13: Effect of velocity slip on induced magnetic field

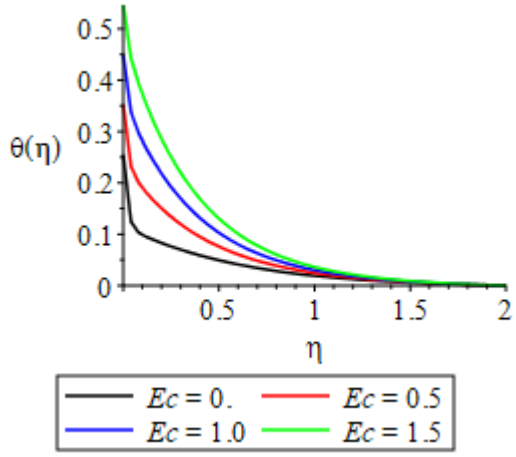

Figure 14: Effect of Eckert number on temperature distribution

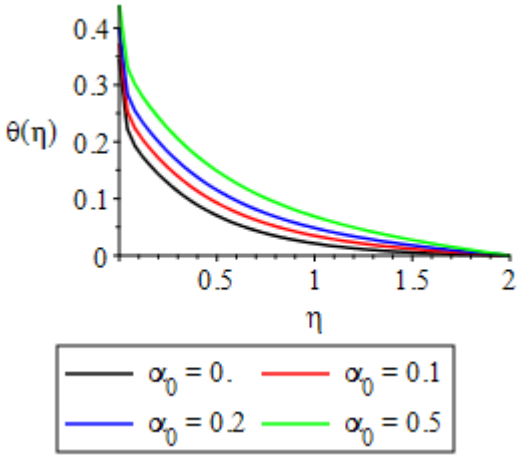

Figure 15: Effect of magnetic parameter on temperature distribution

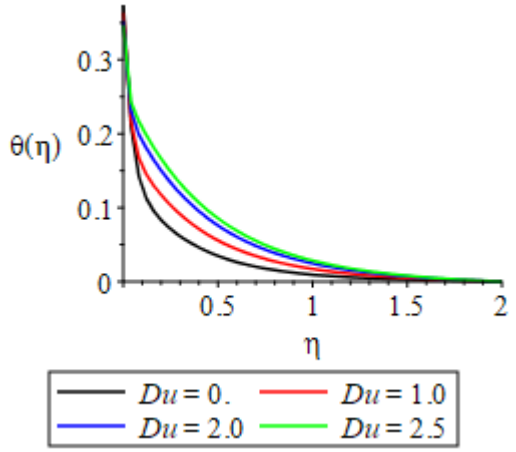

Figure 16: Effect of Dufort number on temperature distribution

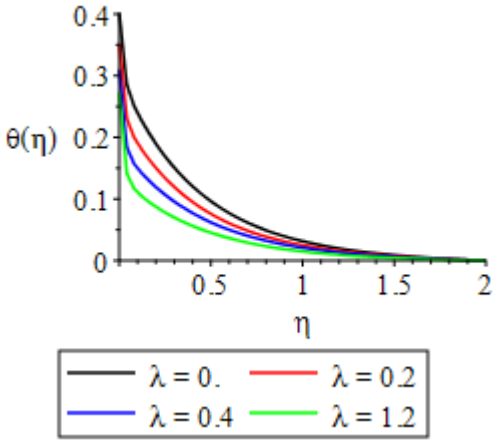

Figure 17: Effect of stretching velocity on temperature distribution

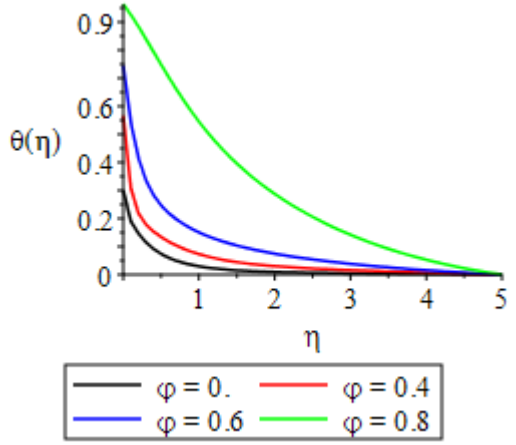

Figure 18: Effect of nanofluid parameter on temperature distribution

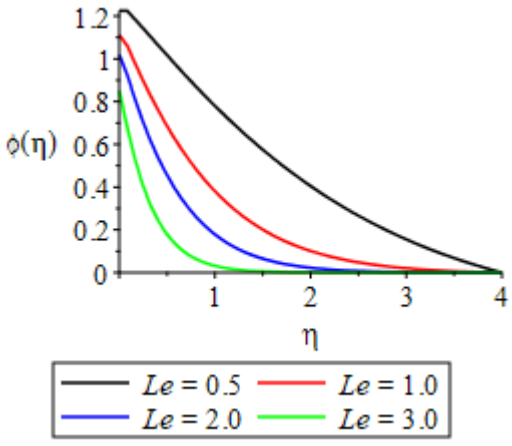

Figure 19: Effect of Lewis number on concentration distribution

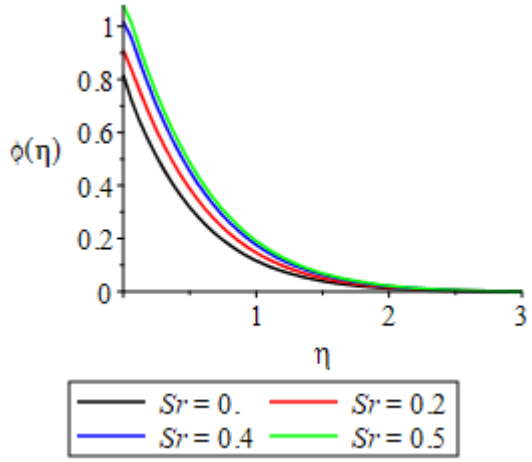

Figure20: Effect of Soret number on concentration distribution

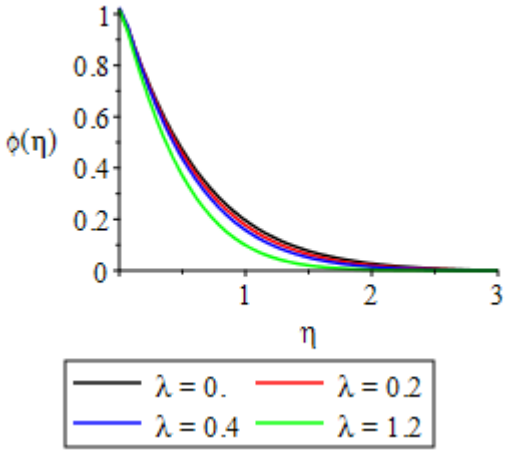

Figure 21: Effect of stretching velocity on concentration distribution

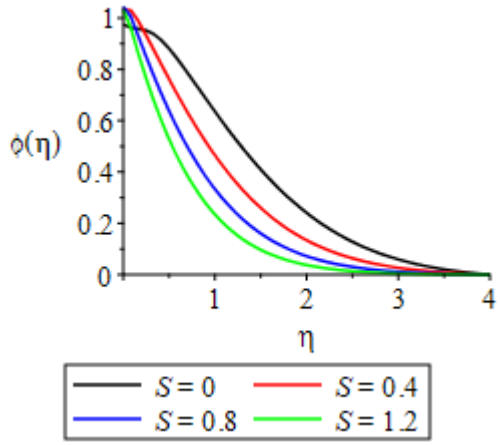

Figure 22: Effect of suction velocity on concentration distribution

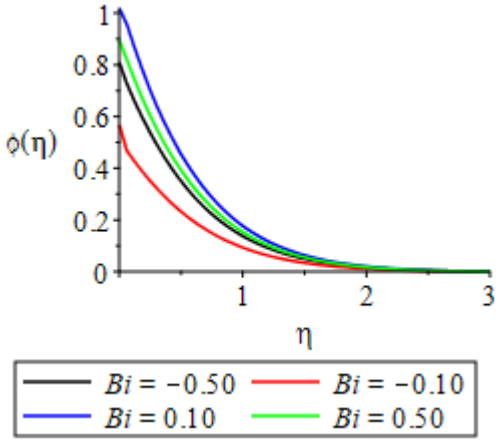

Figure 23: Effect of convective heat transfer on concentration distribution

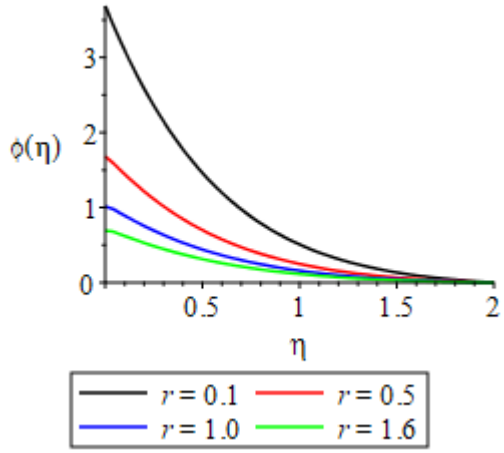

Figure 24: Effect of concentration slip on concentration distribution

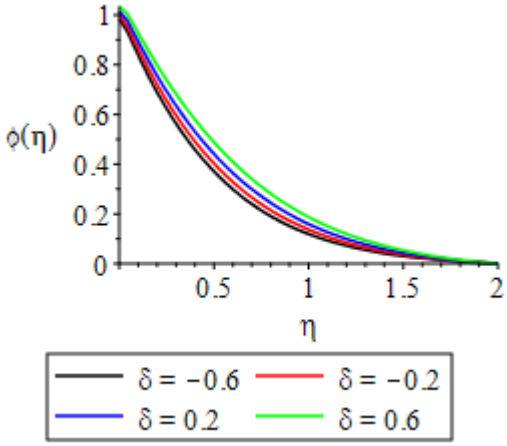

Figure 25: Effect of reactivity parameter on concentration distribution

5. Conclusion

Homotopy Analysis Method (HAM) that uses the homotopy parameter that split nonlinear system into an infinite set of linear systems has been used, while the continuation methods require solving a discrete linear system as the homotopy parameter is varied to solve the nonlinear system. The procedure that generates the

result numerically and graphed is codded in Wolfram mathematical language. The result of the procedure is represented both in figures and tables. From the discussion above, some of the results obtained are:

- velocity increases as stretching velocity increases.
- at a higher stretching velocity, velocity close to the surface is higher that the velocity at the surface.
- velocity boundary layer increase with increase in stretching velocity.
- both buoyancy ratio and Grashof (thermal) increases the velocity distributions
- Eckert number, magnetic parameter, Dufort number and nanofluid parameter were observed to enhances the temperature distributions.
- close to the surface of flow, temperature dropped rapidly and the approaches zero asymptotically.
- that concentration boundary layer decline as Lewis number increases
- that concentration flux at the surface depends on the values of Lewis number.
- stretching velocity declines the concentration
- suction velocity and concentration slip bring about decline in concentration of the flow field as displayed suction or slip have the tendencies of reducing the chemical species in the flow field leaving behind less concentration.
- that when heat moves from solid surface to fluid ($Bi < 0$) the temperature of the fluid flow increases
- reactivity parameter of the chemical species was seen to increase the species concentration for the case of generative chemical reaction and decline the concentration boundary layer for destructive reaction.
- that unsteadiness parameter, thermophoretic parameter β, radiation, reaction order, Dufort number Du and magnetic inductance κ, decline skin-friction of the flow
- Soret number, Magnetic Prandtl number, stretching velocity, buoyancy ratio, Grashof number, magnetic inductance, nanofluid parameter, and reactivity parameter enhances the skin-friction.
- that slip velocity increases skin-friction and Nusselt number and decline Sherwood number of the flow field.
- Increases in Suction velocity decreases skin-friction and Nusselt number,
- while increases in Nanofluid parameter increases the skin friction and Nusselt number and

Disclosure

O. A. Akinyemi, R. E. Asibor and A.M. Okedoye permanent address is as follows: Department of Mathematics, Federal University of Petroleum Resources, Effurun, Delta State, Nigeria, Department of Computer Science/Mathematics, Igbinedion University Okada, Edo State, Nigeria and Department of Mathematics, Federal University of Petroleum Resources, Effurun, Delta State, Nigeria respectively

Conflicts of Interest

The authors declare that there are no conflicts of interest regarding the publication of this article.

Acknowledgments

The authors would like to express their gratitude to Covenant University, Ota, Ogun State, for providing enabling environment and research facilities.

References

[1]. Rajput, G.R., Shamshuddin, M.D., and Salawu, S.O., Thermo Solutal Convective Non-Newtonian Radiative Casson Fluid Transport in a Vertical Plate Propagated by Arrhenius Kinetics with Heat Source/Sink, *Heat Transf.*, vol. 20, pp. 1–20, 2020.

[2]. Salawu, S.O., Fatunmbi, E.O., and Ayanshola, M.A., On the Reactive Diffusion of a Fourth-Grade Hydromagnetic Fluid Flow and Thermal Criticality in a Plane Couette Device, *Results Eng.*, vol. 8, p. 100169, 2020a.

[3]. Cimpean, S.D. and Pop, I., Fully Developed Mixed Convection Flow of a Nanofluid through an Inclined Channel Filled with a Porous Medium, *Int. J. Heat Mass Transf.*, vol. 55, pp. 907–914, 2012.

[4]. Ganji, D.D., Habibollah, S., and Kachapi, H., Natural, Mixed, and Forced Convection in Nanofluid, *Anal. Meth. Appl. Micro Nano Technol.*, vol. 15, pp. 205–269, 2015.

[5]. Shamshuddin, M.D. and Sheri, S.R., Free Convection from a Rotating Vertical Porous Plate in a Dissipative Micropolar Fluid with Cross Diffusion Effects, *Adv. Model. Anal. A*, vol. 86, pp. 627–657, 2017.

[6]. Madhu, M., Mahanthesh, B., Shashikumar, N.S., Shehzad, S.A., Khan, S.U., and Gireesha, B.J., Performance of Second Law in Carreau Fluid Flow by an Inclined Microchannel with Radiative Heated Convective Condition, *Int. Commun. Heat Mass Transf.*, vol. 117, p. 104761, 2020.
[7]. Devi, S.P.A. and Thiyagarajan, M., Steady Nonlinear Hydromagnetic Flow and Heat Transfer over a Stretching Surface of Variable Temperature, *Heat Mass Transf.*, vol. 42, pp. 671–677, 2006.
[8]. Aziz, A. and Khan, W.A., Natural Convective Boundary Layer Flow of a Nanofluid past a Convectively Heated Vertical Plate, *Int. J. Therm. Sci.*, vol. 52, pp. 83–90, 2012.
[9]. Mustafa, M., Hayat, T., Pop, I., Asghar, S., and Obaidat, S., Stagnation-Point Flow of a Nanofluid towards a Stretching Sheet, *Int. J. Heat Mass Transf.*, vol. 54, pp. 5588–5594, 2011.
[10]. Okedoye, A.M., Unsteady MHD Mixed Convection Flow past an Oscillating Plate with Heat Source/Sink, *J. Naval Architect. Marine Eng.*, vol. 11, pp. 167–176, 2014.
[11]. Jamalabadi, M.Y.A., Ghasemi, M., Alamian, R., Wongwises, S., Afrand, M., and Shadloo, M.S., Modeling of Subcooled Flow Boiling with Nanoparticles under the Influence of a Magnetic Field, *Symmetry*, vol. 11, p. 1275, 2019.
[12]. Khan, M., Karim, I., Islam, M., and Wahiduzzaman, M., MHD Boundary Layer Radiative, Heat Generating and Chemical Reacting Flow past a Wedge Moving in a Nanofluid, *Nano Converg.*, vol. 10, pp. 20–28, 2014.
[13]. Mabood, F., Ibrahim, S.M., Rashidi, M.M., Shadloo, M.S., and Lorenzini, G., Non-Uniform Heat Source/Sink and Soret Effects on MHD Non-Darcian Convective Flow past a Stretching Sheet in a Micropolar Fluid with Radiation, *Int. J. Heat Mass Transf.*, vol. 93, pp. 674–682, 2016.
[14]. Haritha, A., Devasena, Y., and Vishali, B., MHD Heat and Mass Transfer of the Unsteady Flow of a Maxwell Fluid over a Stretching Surface with Navier Slip and Convective Boundary Conditions, *Glob, J. Pure Appl. Math.*, vol. 13, pp. 2169–2179, 2017.
[15]. Zeb, H., Wahab, H.A., Shahzad, M., Bhatti, S., and Gulistan, M., Thermal Effects on MHD Unsteady Newtonian Fluid Flow over a Stretching Sheet, *J. Nanofluids*, vol. 7, pp. 704–710, 2018.
[16]. Akindele M. Okedoye1, Sulyman O. Salawu (2020): transient heat and mass transfer of hydromagnetic effects on the flow past a porous medium with movable vertical permeablesheet. *Int. J. of Applied Mechanics and Engineering, 2020, vol.25, No.4, pp.175-190.* DOI: 10.2478/ijame-2020-0057
[17]. Sajid, T., Tanveer, S., Sabir, J., and Guirao, L.G., Impact of Activation Energy and Temperature-Dependent Heat Source/Sink on Maxwell–Sutter by Fluid, *Math. Prob. Eng.*, vol. 20, p. 5251804, 2020.
[18]. Salawu, S.O. and Ogunseye, H.A., Entropy Generation of a Radiative Hydromagnetic Powell–Eyring Chemical Reaction Nanofluid with Variable Conductivity and Electric Field Loading, *Results Eng.*, vol. 5, p. 100072, 2002.
[19]. Mosavati, B., Mosavati, M., and Kowsary, F., Solution of Radiative Inverse Boundary Design Problem in a Combined RadiatingFree Convecting Furnace, *Int. Commun. Heat Mass Transf.*, vol. 45, pp. 130–136, 2013.
[20]. Mosavati, B., Mosavati, M., and Kowsary, F., Inverse Boundary Design Solution in a Combined Radiating-Free Convecting Furnace Filled with Participating Medium Containing Specularly Reflecting Walls, *Int. Commun. Heat Mass Transf.*, vol. 76, pp. 69–76, 2016.
[21]. Reddy, J.V.R., Sugunamma, V., and Sandeep, N., Simultaneous Impacts of Joule Heating and Variable Heat Source/Sink on MHD 3D Flow of Carreau-Nanoliquids with Temperature Dependent Viscosity, *Nonlin. Eng.*, vol. 8, no. 1, pp. 356–367, 2018.
[22]. Patil, P.M., Kumbarwadi, N., and Shashikant, A., Effects of MHD Mixed Convection with Non-Uniform Heat Source/Sink and Cross Diffusion over Exponentially Stretching Sheet, *Int. J. Numer. Meth. Heat Fluid Flow*, vol. 28, pp. 273–281, 2018.
[23]. Salawu, S.O. and Dada, M.S., Lie Group Analysis of Soret and Dufour Effects on Radiative Inclined Magnetic Pressure-Driven Flow past a Darcy–Forchheimer Medium, *J. Serbian Soc. Comput. Mech.*, vol. 12, no. 1, pp. 108–125, 2018.
[24]. Thriveni, K. and Mahanthesh, B., Sensitivity Analysis of Nonlinear Radiated Heat Transport of Hybrid Nanoliquid in an Annulus Subjected to the Nonlinear Boussinesq Approximation, *J. Therm. Anal. Calorim.*, vol. 25, p. 459, 2020a.
[25]. Thriveni, K. and Mahanthesh, B., Nonlinear Boussinesq Buoyancy Driven Flow and Radiative Heat Transport of Magnetohybrid Nanoliquid in an Annulus: A Statistical Framework, *Heat Transf.*, vol. 6, pp. 1–24, 2020b.

[26]. Yousif, M.A., Ismael, H.F., Abbas, T., and Ellahi, R., Numerical Study of Momentum and Heat Transfer of MHD Carreau Nanofluid over an Exponentially Stretched Plate with Internal Heat Source/Sink and Radiation, *Heat Transf. Res.*, vol. 50, no. 7, pp. 649–658, 2019.
[27]. Shamshuddin, M.D., Mishra, S.R., and B´eg, O.A., Lie Symmetry Analysis and Numerical Solutions for Thermo-Solutal Chemically Reacting Radiative Micropolar Flow from an Inclined Porous Plate, *Heat Transf. Asian Res.*, vol. 47, no. 5, pp. 918–940, 2018.
[28]. Salawu, S.O., Oderinu, R.A., and Ohaegbue, A.D., Thermal Runaway and Thermodynamic Second Law of a Reactive Couple Stress Fluid with Variable Properties and Navier Slips, *Sci. African*, vol. 7, p. e00261, 2020c.
[29]. Ogunseye, H.A., Salawu, S.O., Tijani, Y.O., Riliwan, M., and Sibanda, P., Dynamical Analysis of Hydromagnetic Brownian and Thermophoresis Effects of Squeezing Eyring–Powell Nanofluid Flow with Variable Thermal Conductivity and Chemical Reaction, *Multidisc. Model. Mater. Struct.*, vol. 15, no. 6, pp. 1100–1120, 2019.
[30]. Mustafa, M., Khan, J.A., Hayat, T., and Alsaedi, A., Buoyancy Effects on the MHD Nanofluid Flow past a Vertical Surface with Chemical Reaction and Activation Energy, *Int. J. Heat Mass Transf.*, vol. 108, pp. 1340–1346, 2017.
[31]. Khan, M.I., Qayyum, S., Hayat, T., and Waqas, M., Entropy Generation Minimization and Binary Chemical Reaction with Arrhenius Activation Energy in MHD Radiative Flow of Nanomaterial, *J. Mol. Liq.*, vol. 259, pp. 274–283, 2018.
[32]. Azam, M., Xu, M., Shakoor, T., and Khan, M., Effects of Arrhenius Activation Energy in Developing of Covalent Bonding in Axisymmetric Flow of Radiative-Cross Nanofluid, *Int. Commun. Heat Mass Transf.*, vol. 113, p. 104547, 2020.
[33]. B´eg, O.A., Kuharat, S., Ferdows, M., Das, M., and Kadir, A., Shamshuddin, M.D., Modelling Magnetic Nanopolymer Flow with Induction and Nanoparticle Solid Volume Fraction Effects: Solar Magnetic Nanopolymer Fabrication Volume Fraction, *I Mech E Part N: J. Nanomater. Nanoeng. Nanosyst.*, vol. 233, pp. 27–45, 2019.
[34]. Waqas, H., Khan, S.U., Shehzad, S.A., and Imran, M., Radiative Flow of Maxwell Nanofluid Containing Gyrotactic Microorganism and Energy Activation with Convective Nield Conditions, *Heat Transf. Asian Res.*, vol. 48, pp. 1663–1687, 2019.
[35]. Hayat, T., Ullah, I., Waqas, M., and Alsaedi, A., Attributes of Activation Energy and Exponential Based Heat Source in Flow of Carreau Fluid with Cross-Diffusion Effects, *J. Non-Equilib. Thermodyn.*, vol. 18, pp. 203–213, 2019.
[36]. Salawu, S.O. and Disu, A.B., Branch-Chain Criticality and Explosion for a Generalized Thermal Oldroyd 6-Constant Couette Reactive Fluid Flow, *South African J. Chem. Eng.*, vol. 34, pp. 90–96, 2020.
[37]. Akindele M. Okedoye1, Sulyman O. Salawu (2019): effect of nonlinear radiative heat and mass transfer on MHD flow over a stretching surface with variable conductivity and viscosity. Journal of the Serbian Society for Computational Mechanics / Vol. 13 / No. 2, 2019 / pp 86-103 (10.24874/jsscm.2019.13.02.07)
[38]. *Akindele M. Okedoye,1 Sulyman O. Salawu,2,∗ & Raphael E. Asibor* (2021): A convective MHD double diffusive flow of a binary mixture through an isothermal and porous moving plate with activation energy. *Computational Thermal Sciences*, 13(5):45–60 (2021)
[39]. Mohamed Abd El-Aziz 1 and Ahmed A. Afify (2018): Influences of Slip Velocity and Induced Magnetic Field on MHD Stagnation-Point Flow and Heat Transfer of Casson Fluid over a Stretching Sheet. Mathematical Problems in Engineering Volume 2018, Article ID 9402836, 11 pages https://doi.org/10.1155/2018/9402836